Power Electronic Systems
Laboratory

IEEE Transactions on Magnetics, Vol. 52, No. 7, July 2016

Characterization of Electromagnetic Rotor Material Properties and Their Impact on an Ultra-High Speed Spinning Ball Motor

M. Schuck,
T. Nussbaumer,
J. W. Kolar

Eidgenössische Technische Hochschule Zürich
Swiss Federal Institute of Technology Zurich

Characterization of Electromagnetic Rotor Material Properties and Their Impact on an Ultra-High Speed Spinning Ball Motor

Marcel Schuck[1], Thomas Nussbaumer[2], and Johann W. Kolar[1], *Fellow, IEEE*

[1]Power Electronic Systems Laboratory, Swiss Federal Institute of Technology, Zürich 8092, Switzerland
[2]Levitronix GmbH, Zürich 8005, Switzerland

The ongoing miniaturization trend of electric machines increases the demand for higher rotational speeds to provide a required power level at decreased size. In this paper, new concepts for bearingless machines with ultra-high rotational speeds exceeding 25 million rotations per minute are researched. While the mechanical properties of the employed sub-millimeter-sized spherical steel rotors are documented, insufficient information is available on the electromagnetic characteristics that are crucial for magnetic levitation and acceleration. This paper outlines the relations between the relative permeability and conductivity of the rotor material and the achievable active magnetic bearing force and angular acceleration. Measured results for complete hysteresis curves of different rotor steels are presented.

***Index Terms*—Asynchronous machine, magnetic bearing, material characterization, spinning ball, ultra-high speed.**

I. Introduction

INCREASING the rotational speed of an electric machine allows the achievement of a required power level at a decreased size, which has led to an ongoing miniaturization trend of machines with rising rotational speeds. The latter can be achieved by reducing bearing friction, which can be effectively facilitated using magnetic bearings. Drive systems with rotational speeds of up to 1 million rotations per minute (r/min) have been developed in the past [1]. By significantly reducing other losses that become significant at high rotational speeds, such as air friction, rotational speeds exceeding 20 million r/min can be achieved. The highest reported rotational speed of 23.16 million r/min was achieved with a steel sphere of 0.8 mm in diameter, which was magnetically levitated inside a vacuum tube and eventually destroyed due to the centrifugal load [2]. Since then, such high rotational speeds have not been achieved in other more recently reported attempts [3].

In this paper, new concepts for drives with ultra-high rotational speeds beyond 25 million r/min are researched in order to extend the limits of conventional machines and overcome the challenges with regard to power density, mechanical stress, and controllability of highly dynamic systems. The ultimate limit of the rotational speed is determined by the centrifugal load of the rotor. Therefore, small spherical rotors with diameters of less than 1 mm made from ferromagnetic and conductive materials with high tensile strengths are used.

Small spheres made from various martensitic chrome steels and tungsten-carbide cobalt are used in ball bearings and are, therefore, readily available. The available characteristic data for these spheres is mostly limited to their mechanical properties in the aforementioned application, while insufficient information is available on the electromagnetic characteristics of the different materials. Yet, the latter are critical to assessing the achievable performance of the magnetic bearing and drive in the ultra-high speed motor application at hand. In this paper, the analytic models of the motor drive and magnetic bearing are provided and characteristic magnetic properties for different materials are obtained through measurements.

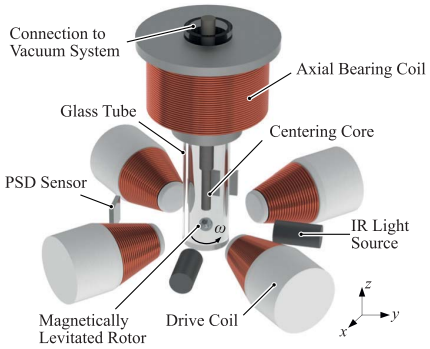

Fig. 1. Setup of the ultra-high speed motor.

Section II briefly describes the motor setup. In Section III, analytic models for the achievable active magnetic bearing (AMB) force and motor torque, dependent on the relative permeability and conductivity of the rotor material, are derived. The aforementioned material properties were obtained experimentally through measuring complete hysteresis curves of different materials by directly using the spherical rotors as specimens in a vibrating sample magnetometer (VSM). The obtained results are presented in Section IV.

II. Motor Setup

The developed ultra-high speed motor setup is shown in Fig. 1. The rotor is placed inside an evacuated glass tube to minimize air friction. Bearing friction is eliminated using an axial magnetic bearing, which is constructed from a copper coil wound around a hollow ferromagnetic core to allow sufficient space for inserting the vacuum tube through the core. A second, solid ferromagnetic cylinder is placed directly inside the vacuum tube to act as a centering core that concentrates the magnetic flux and is the center of attraction for the levitated rotor.

In addition to the axial bearing, four air coils are placed radially around the rotor to produce the fast rotational magnetic fields required for torque generation. Acceleration is achieved by the principle of a solid rotor induction machine, where

Manuscript received November 6, 2015; revised January 10, 2016; accepted February 3, 2016. Date of publication February 11, 2016; date of current version June 22, 2016. Corresponding author: M. Schuck (e-mail: schuck@lem.ee.ethz.ch).

Color versions of one or more of the figures in this paper are available online at http://ieeexplore.ieee.org.

Digital Object Identifier 10.1109/TMAG.2016.2529498

eddy currents are induced inside the rotor, which are subject to tangential Lorentz forces.

As there is almost no air friction that acts upon the rotor, radial oscillations due to disturbances are weakly damped, causing the magnetic suspension to become unstable. Therefore, the radially placed coils are also used as actuators for a radial AMB, which increases radial damping of the system.

For the magnetic suspension to operate properly, the axial and radial rotor positions have to be measured and controlled continuously. In the developed setup, the rotor is illuminated by two orthogonally placed infrared light sources resulting in a rotor shadow being drawn onto two 2-D position-sensitive device sensors, which are placed on the opposite side of the vacuum glass tube. The resulting position signals are fed into digital controllers, which regulate the rotor position by adjusting the currents in the axial and radial bearing coils.

With the developed setup, spherical rotors with diameters of 3 mm down to sub-millimeter sizes can be levitated and accelerated.

III. Influence of Material Properties on Bearing and Drive Performance

To assess the influence of the characteristic rotor material parameters on the achievable magnetic bearing and drive performance of the ultra-high speed motor, analytic models for the achievable AMB force and motor torque are derived below.

A. Magnetic Bearing

Introducing a body made from a magnetizable material, which is not a permanent magnet, into the external magnetic field $\vec{H}_{\text{ext}}$ with the magnetic induction $\vec{B}_{\text{ext}} = \mu_0 \vec{H}_{\text{ext}}$ as generated by the bearing coil results in magnetization $\vec{M}$ of this body. The latter is dependent on the value of $\vec{H}_{\text{ext}}$ and the magnetic properties of the rotor material as characterized by its B-H curve and results in a force that originates from the interaction with the external induction $\vec{B}_{\text{ext}}$. The influence of the magnetic properties of the rotor material on the achievable AMB force is studied by applying magnetostatic principles. To provide analytic expressions, two simplifying assumptions are introduced, which have been verified by 2-D and 3-D finite-element-method magnetic simulations to not have a negative effect on the accuracy of the developed force model.

1) The magnetization $\vec{M}$ of the sphere is uniform and is caused by the magnitude of the external magnetic induction $|\vec{B}_{\text{ext}}|$ at its center ($z = z_0$).
2) The magnitude of the external magnetic induction varies linearly over the diameter of the sphere, with its gradient being determined by $(\partial|\vec{B}_{\text{ext}}(z_0)|/\partial z)$.

In order to determine the bearing force, the magnetization and magnetic induction inside the sphere, as caused by the external magnetic induction, must be determined first. For a sphere with uniform magnetization of magnitude M_0, as shown in Fig. 2, without an external magnetic field, the magnetic scalar potential in spherical coordinates can be obtained as [4]

$$\Phi_{M,\text{in}} = \frac{1}{3} M_0 r \cos(\theta) \quad \Phi_{M,\text{out}} = \frac{1}{3} M_0 a^3 \frac{1}{r^2} \cos(\theta) \tag{1}$$

where a denotes the radius of the sphere. Consequently, the magnetic field and magnetic induction inside the sphere are

$$\vec{H}_{\text{in}} = -\frac{1}{3}\vec{M} \qquad \vec{B}_{\text{in}} = \mu_0(\vec{H}_{\text{in}} + \vec{M}) = \frac{2\mu_0}{3}\vec{M}. \tag{2}$$

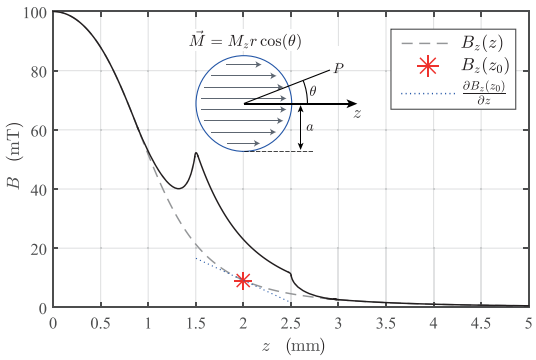

Fig. 2. Magnitude of the magnetic induction inside and outside of the sphere for varying distances from the AMB coil.

To obtain the field inside a magnetized sphere placed in an external magnetic induction $\vec{B}_{\text{ext}} = \mu_0 \vec{H}_{\text{ext}}$, the field components of (2) are superimposed with the external field, yielding

$$\vec{H}_{\text{in}} = \frac{1}{\mu_0}\vec{B}_{\text{ext}} - \frac{1}{3}\vec{M} \qquad \vec{B}_{\text{in}} = \vec{B}_{\text{ext}} + \frac{2\mu_0}{3}\vec{M}. \tag{3}$$

From this, a general expression for the magnetic induction inside the sphere dependent on the external magnetic induction can be found by eliminating $\vec{M}$ as

$$\vec{B}_{\text{in}} + 2\mu_0 \vec{H}_{\text{in}} = 3\vec{B}_{\text{ext}} \tag{4}$$

where the B-H curve of the rotor material relates $\vec{B}_{\text{in}}$ and $\vec{H}_{\text{in}}$ as $\vec{B}_{\text{in}} = \mu(|\vec{H}_{\text{in}}|)\vec{H}_{\text{in}}$ for isotropic materials. The resulting magnetic induction inside and outside the rotor are shown in Fig. 2 for a sphere that has been introduced into the field of a cylindrical bearing coil, where z denotes the distance from the coil. The scaling of the field inside the rotor is clearly visible and the relevant variables for the subsequent force calculation are marked. In the absence of macroscopic conduction currents, the total magnetic force acting on a body with magnetization $\vec{M}$ and volume V, which is bounded by a surface S, can be obtained from the elementary force law as

$$\vec{F} = \int_V \rho_M \vec{B}_{\text{ext}} dV + \int_S \sigma_M \vec{B}_{\text{ext}} dS \tag{5}$$

where $\vec{B}_{\text{ext}}$ denotes the applied magnetic induction, not including that of the body for which the force is calculated. The concept has been employed that a magnetization $\vec{M}$ is equivalent to a volume current density $\vec{J}_M = (\vec{\nabla} \times \vec{M})$ and a surface current density $\vec{K}_M = (\vec{M} \times \vec{n})$. The magnetic volume charge density and magnetic surface charge density, which are used as mathematical equivalents to electric charges, are denoted by $\rho_M = -\vec{\nabla} \cdot \vec{M}$ and $\sigma_M = \vec{M} \cdot \vec{n}$, respectively. Assuming a uniform magnetization inside the sphere yields $\rho_M = 0$, and the first term in (5) becomes zero. Based on the uniform magnetization, the magnetic surface charge is obtained as $\sigma_M = M_z \cos(\theta)$. Including the assumptions stated above, the external magnetic induction can be parameterized in spherical coordinates as

$$\vec{B}_{\text{ext}} = \begin{pmatrix} B_r r \sin(\theta) \\ 0 \\ B_z(z_0) + \frac{\partial B_z(z_0)}{\partial z} r \cos(\theta) \end{pmatrix} \tag{6}$$

where B_r and $B_z(z_0)$ denote the radial component and the axial component at the center position of the sphere of the magnetic

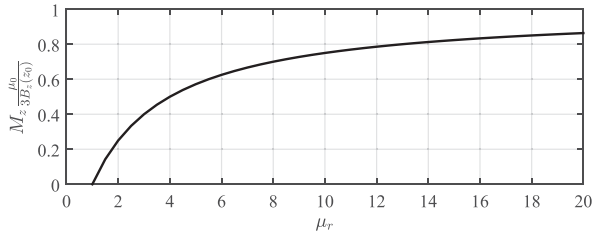

Fig. 3. Normalized magnetization of the sphere for different values of μ_r.

induction, respectively. By inserting (6) into (5), the resulting force is obtained as

$$\vec{F} = \frac{4}{3}\pi a^3 M_z \frac{\partial B_z(z_0)}{\partial z}\vec{e}_z. \tag{7}$$

As the magnetization of the sphere is directed into the same direction as the external magnetic induction, the resulting force is always directed toward the bearing coil, and its magnitude is dependent on the gradient of the external magnetic induction in z-direction. It is independent of the radial component B_r, which can, therefore, be chosen arbitrarily in the parameterization of the field. The absolute value of the external field only affects the magnetization M_z of the sphere. If the relative magnetic permeability μ_r is assumed to be constant and hysteresis effects are neglected, (3) can be used to obtain an analytic expression for the magnetization as

$$M_z = \frac{3}{\mu_0}\left(\frac{\mu_r - 1}{\mu_r + 2}\right) B_z(z_0). \tag{8}$$

It is shown in Section IV that the aforementioned assumptions are well justified for suitable rotor materials. The presence of hysteresis is undesired in the considered AMB, as the resulting remanent magnetization in the absence of an external magnetic induction can cause undesired residual forces acting between the rotor and ferromagnetic parts of the AMB system. By inserting (8) into (7), it is apparent that, for given values of $B_z(z_0)$ with the gradient of the induction, the force increases rapidly for small increasing values of μ_r, while it levels off at high μ_r values. This behavior is shown in Fig. 3, where the normalized magnetization is plotted for different values of μ_r. Moreover, from the analytic expressions, it can be observed that the conductivity of the rotor material has no effect on the achievable magnetic force.

B. Torque Generation

A high torque is desirable to achieve fast acceleration of the rotor. The motor torque is generated by the interaction of the fast rotating magnetic field as generated by the drive coils with the induced eddy currents inside the rotor. A detailed analysis has been presented in [5], from which the influence of the rotor material properties on the drive performance can be studied. The general expression for the torque is derived as

$$\vec{T} = \underbrace{\frac{3\pi a^3}{1+\sqrt{2}}\frac{B_{\text{rot}}^2}{\mu_0}}_{T_{\text{bd}}} \underbrace{\frac{2+\sqrt{2}}{\sqrt{2}+q+\frac{1}{q}}}_{\xi}\vec{e}_z \tag{9}$$

where B_{rot} denotes the magnitude of the magnetic flux density used for torque generation, which is oriented in radial direction, and the sphere rotates around the z-axis. The breakdown torque denoted by T_{bd} is the maximum achievable torque for a given rotor radius and magnetic flux density. The factor q

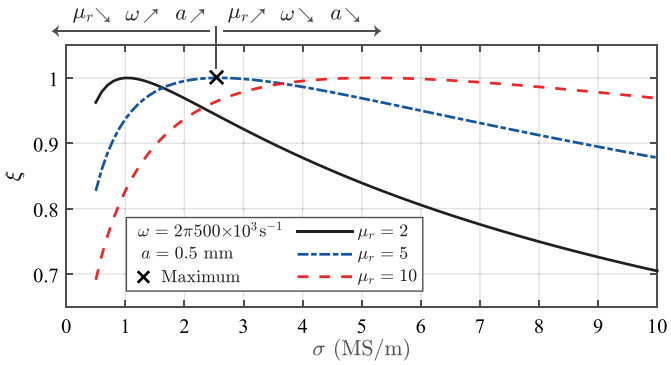

Fig. 4. Value of the breakdown torque scaling factor of (9) dependent on σ, μ_r, ω, and a.

TABLE I
ELECTROMAGNETIC PROPERTIES OF DIFFERENT ROTOR MATERIALS

Material Number	ρ / kg/dm^3	σ / MS/m	μ_r (measured)
100Cr6	~ 7.9	~ 4.6	4.13
X65Cr13	~ 7.7	~ 1.8	4.14
X47Cr14	~ 7.7	~ 1.8	4.12
X46Cr13	~ 7.7	~ 1.8	4.17
X105CrMo17	~ 7.7	~ 1.3	4.09
TC3	~ 14.2	-	3.46
TC2	~ 14.9	-	4.47

in (9) contains the variables corresponding to the properties of the rotor material and is given as

$$q = \frac{1}{a}\sqrt{\frac{\mu_r}{\mu_0 \sigma \omega}} \tag{10}$$

where σ and ω denote the electrical conductivity and the slip frequency, respectively. The latter is the difference between the frequency of the rotating magnetic field and the rotor spinning frequency. T_{bd} is obtained for $q = 1$ ($\xi = 1$) and the achievable torque is dependent on the combination of μ_r, σ, and ω, rather than on a single material property alone. It can be seen that the peak value of the scaling factor ξ is shifted based on the dependences as shown in Fig. 4.

IV. ROTOR MATERIAL CHARACTERIZATION

To assess the suitability of different rotor materials for magnetic levitation and acceleration in the ultra-high speed motor based on the analytic relations provided in Section III, the relevant material properties were obtained through measurements. Spheres of small diameters are readily available, as they are commonly used in ball bearings. Table I lists common conductive materials with ferromagnetic behavior and their properties relevant to this paper, where ρ denotes the density of the material. The detailed compositions of the materials are standardized and can be found in the respective material datasheets as well as in [6] and are not reproduced here. While the conductivity of the material is usually given, insufficient information is available on its relative magnetic permeability. Therefore, the complete magnetization curves have been obtained through measurements, which were carried out using a VSM [7]–[9]. The advantage of this method is that the rotors can directly be used as specimens in an open circuit measurement, which allows material changes due to machining and thermal treatment [10] to be taken into consideration. Like the material composition, the machining process and thermal treatment of the different sphere materials, which induce compressive residual stresses in the rotors,

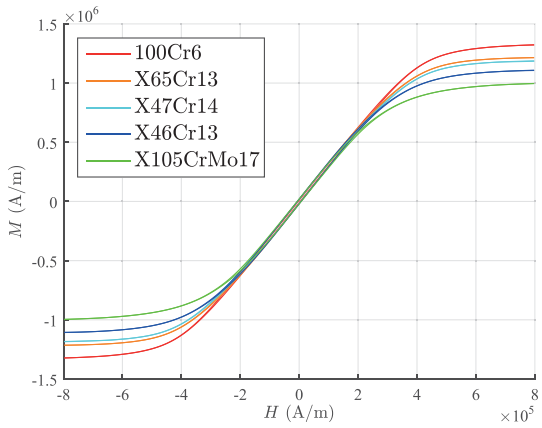

Fig. 5. Measured magnetization curves of materials in group 1.

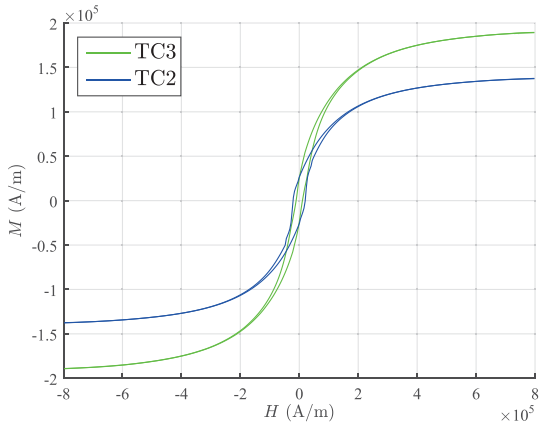

Fig. 6. Measured magnetization curves of materials in group 2.

follow standardized procedures [6]. Therefore, the results, as obtained from the measured samples, are valid across sizes, batches, and manufacturers and are widely applicable to steel spheres made from the considered material. The measurements were carried out with spheres of 0.5–1.4 mm in diameter, yielding sample weights in the range of several milligrams. Accurate results can be obtained as the instrument is calibrated with a spherical reference sample (e.g., chemically pure Ni $d = 1$ mm; see [11]), which omits the necessity of compensating for the actual sample geometry affecting the measurement results [12], [13].

The rotor materials exhibit isotropic behavior regarding their magnetic properties, which was verified by repeated measurements after rotating the sample by 90°. Due to the operating principle of the VSM, the magnetic moment $\vec{m}$ of the sample as a function of the applied magnetic field $\vec{H}$ is measured. If the specimen consists of an isotropic material, the magnetization M is obtained by dividing m by the volume of the sample. As the local μ_r of a material corresponds to the slope of the measured magnetization curve, it is calculated as

$$\mu_r = \frac{dM}{dH} + 1 \tag{11}$$

where H is known from the measurements.

Figs. 5 and 6 show the measured hysteresis curves for all listed materials of Table I, and the values of the initial relative permeability (μ_r at $H = 0$) have been added to Table I. It can be observed (Fig. 5) that the martensitic chrome steels denoted by the EN material numbers 100Cr6, X65Cr13, X47Cr14, X46Cr13, and X105CrMo17 (group 1) exhibit very similar behaviors regarding the initial values of μ_r with a narrow hysteresis loop as desired, and differ only in the magnetization at saturation. Contrarily, the materials TC3 and TC2 (group 2) exhibit significantly different behaviors with wider hysteresis loops and significantly lower values of the saturation magnetization (Fig. 6). This behavior is explicable by their composition, consisting of high percentages of tungsten carbide and cobalt, causing high hardness of these materials. Consequently, the steels in group 1 are equivalently well suited for magnetic levitation, while the materials from group 2 are less suitable as the achievable magnetic bearing forces are significantly lower, according to the analyses as outlined above.

V. Conclusion

Analytic models for assessing the influence of the rotor material on the performance of the magnetic suspension system and the drive of an ultra-high speed motor have been provided. Based on the magnetization curves of various available materials, which have been obtained through measurements and were previously unavailable in the literature, suitable materials were identified. The presented findings are universally applicable and particularly allow the assessment of the suitability of different steels in magnetic bearing applications.

Acknowledgment

This work was supported by the Else & Friedrich Hugel Fund for Mechatronics.

References

[1] C. Zwyssig, J. W. Kolar, and S. D. Round, "Megaspeed drive systems: Pushing beyond 1 million r/min," *IEEE/ASME Trans. Mechatronics*, vol. 14, no. 5, pp. 564–574, Oct. 2009. [Online]. Available: http://ieeexplore.ieee.org/stamp/stamp.jsp?arnumber=481320

[2] J. W. Beams, J. L. Young, III, and J. W. Moore, "The production of high centrifugal fields," *J. Appl. Phys.*, vol. 17, no. 11, pp. 886–890, 1946. [Online]. Available: http://scitation.aip.org/content/aip/journal/jap/17/11/10.1063/1.1707658

[3] A. Boletis and H. Bleuler, "Achieving ultra-high rotating speeds," in *Proc. 8th Int. Symp. Magn. Bearing*, Mito, Japan, Aug. 2002, pp. 539–542.

[4] J. D. Jackson, *Classical Electrodynamics*. New York, NY, USA: Wiley, 1999.

[5] T. Reichert, T. Nussbaumer, and J. W. Kolar, "Complete analytical solution of electromagnetic field problem of high-speed spinning ball," *J. Appl. Phys.*, vol. 112, no. 10, p. 104901, 2012. [Online]. Available: http://scitation.aip.org/content/aip/journal/jap/112/10/10.1063/1.4765676

[6] J. Brändlein, P. Eschmann, L. Hasbargen, and K. Weigand, *Ball and Roller Bearings: Theory, Design and Application*. New York, NY, USA: Wiley, 1999.

[7] S. Foner, "Versatile and sensitive vibrating-sample magnetometer," *Rev. Sci. Instrum.*, vol. 30, no. 7, pp. 548–557, 1959. [Online]. Available: http://scitation.aip.org/content/aip/journal/rsi/30/7/10.1063/1.1716679

[8] S. Tumanski, *Handbook of Magnetic Measurements* (Series in Sensors), 1st ed. Boca Raton, FL, USA: CRC Press, Jun. 2011.

[9] F. Fiorillo, *Characterization and Measurement of Magnetic Materials*, 1st ed. New York, NY, USA:Academic, Feb. 2005.

[10] D. Jiles, *Introduction to Magnetism and Magnetic Materials*. 3rd ed. Boca Raton, FL, USA: CRC Press, 2015.

[11] R. D. Shull, R. D. McMichael, L. J. Swartzendruber, and S. D. Leigh, "Absolute magnetic moment measurements of nickel spheres," *J. Appl. Phys.*, vol. 87, no. 9, pp. 5992–5994, 2000.

[12] A. W. Pacyna and K. Ruebenbauer, "General theory of a vibrating magnetometer with extended coils," *J. Phys. E, Sci. Instrum.*, vol. 17, no. 2, p. 141, 1984.

[13] A. Zieba and S. Foner, "Detection coil, sensitivity function, and sample geometry effects for vibrating sample magnetometers," *Rev. Sci. Instrum.*, vol. 53, no. 9, pp. 1344–1354, 1982.